To be published in "X-Ray Microbeam Technology and Applications,"
Edited by W. Yun, (SPIE Proceedings, Volume 2516, 1995)

Direct observation of microscopic inhomogeneities in high T_c superconductors using energy-dispersive diffraction of synchrotron produced x-rays

E. F. Skelton, S. B. Qadri, M. S. Osofsky, A. R. Drews, and P. R. Broussard
Condensed Matter and Radiation Sciences Division and Materials Science and Technology Division
Naval Research Laboratory, Washington, DC 20375-5000

J. Z. Hu and L. W. Finger
Geophysical Laboratory and Center for High Pressure Research†
Carnegie Institution of Washington, Washington, DC 20015-1305

T. A. Vanderah and D. Kaiser
Ceramics Division, National Institute of Standards and Technology, Gaithersburg, MD 20882

J. L. Peng, S. M. Anlage, and R. L. Greene
Center for Superconductivity Research, Department of Physics
University of Maryland, College Park, MD 20742

J. Giapintzakis
Materials Research Laboratory, University of Illinois, Urbana, IL 61801

ABSTRACT

Evidence of micron-sized structural inhomogeneities in several high transition temperature (T_c) superconductors is presented. By illuminating samples with high energy, highly collimated x-rays produced on a synchrotron wiggler, small changes in the lattice were detected over a spatial scale as small as 10 μm. In the $YBa_2Cu_3O_{7-\delta}$ crystals, these changes are interpreted as evidence of variations in the oxygen content and in the $Nd_{2-x}Ce_xCuO_{4-y}$ crystal, as a variation in the cerium content. Each type of inhomogeneity can affect the superconducting properties.

KEYWORDS: Superconductivity; microdiffraction; synchrotron x-rays; energy-dispersive diffraction; structural inhomogeneities

1. INTRODUCTION

The mechanism of superconductivity in the high temperature superconductors (HTS) is not yet understood. Adding to difficulties in the interpretation of transport data is the fact that single crystals presumed to be structurally and chemically uniform and homogeneous, may not be. One of the few characteristics that is universally accepted about HTS is that their coherence lengths, ξ, are short (on the order of tens of Ångstroms in the Cu-O planes). Since ξ is the decay distance of the superconducting order parameter, sample inhomogeneities, even in single crystals, will strongly affect the measured superconductive properties of the system. These inhomogeneities could be the source of many of the unusual properties that have been reported in HTS. In this paper we present direct evidence of microscopic structural variations which are due to oxygen and cation inhomogeneities in crystals of HTS.

Standard diffraction techniques with conventional x-ray sources represent the classic method for obtaining structural information. This information is limited to a surface region of the sample, as defined by

the penetration depth of the radiation. This depth varies with photon energy and the atomic number of the elements in the sample. Typical skin depths are on the order of a few micrometers. X-ray spot sizes are determined, in part, by the degree to which the radiation from an x-ray generator can be collimated, while retaining an adequate number of photons in the beam to perform the measurement. Typical beam diameters are on the order of millimeters. However, by employing x-rays generated on a synchrotron superconducting wiggler magnet, with its concomitant high energy and low angular dispersion, materials can be probed roughly two orders of magnitude deeper with x-ray beams that are less than 100 μm^2 in cross sectional area. Using such an arrangement, we have detected small compositional and structural variances on spatial scales of a few tens of μm.

2. EXPERIMENTAL PROCEDURES

A schematic diagram of the experimental set up is shown in Fig. 1. All the work reported in this paper was performed on the superconducting wiggler beam line X17C at the National Synchrotron Light Source, Brookhaven National Laboratory. The incident beam entering the experimental hutch is polychromatic, spanning an energy range from a few keV to over 100 keV. It is reduced to a cross section of a few millimeters by aperture controllers in the transport hutch. Once the beam enters the experimental hutch, it is further reduced in cross-section to a dimension 5 μm (horizontal) by 10 μm (vertical). The heavymet blocks used to define the final beam size and position are computer controlled to within a micron. The final beam dimensions are measured by stepping a sharp edge across the beam in 1 micron steps in both the vertical and horizontal directions and monitoring the transmitted beam intensity.

The crystals were mounted on an ω.χ-circle goniometer atop an ω,2θ-stage. The ω.χ-circle was mounted on an *x, y, z*-translation stage. All motions, *x, y, z*, χ, ω, and 2θ, are computer controlled and programmable. Each of the crystals studied in this work were in the approximate shape of a rectangular solid with the largest face normal to the *c*-axis. The longest edge of each crystal was aligned parallel to the *z*-axis (vertical axis) when $\chi = 0$. The *x*-axis is taken to be parallel to the on-going x-ray beam and the *y*-axis is orthogonal to *x* and *z*. (See Fig. 1.)

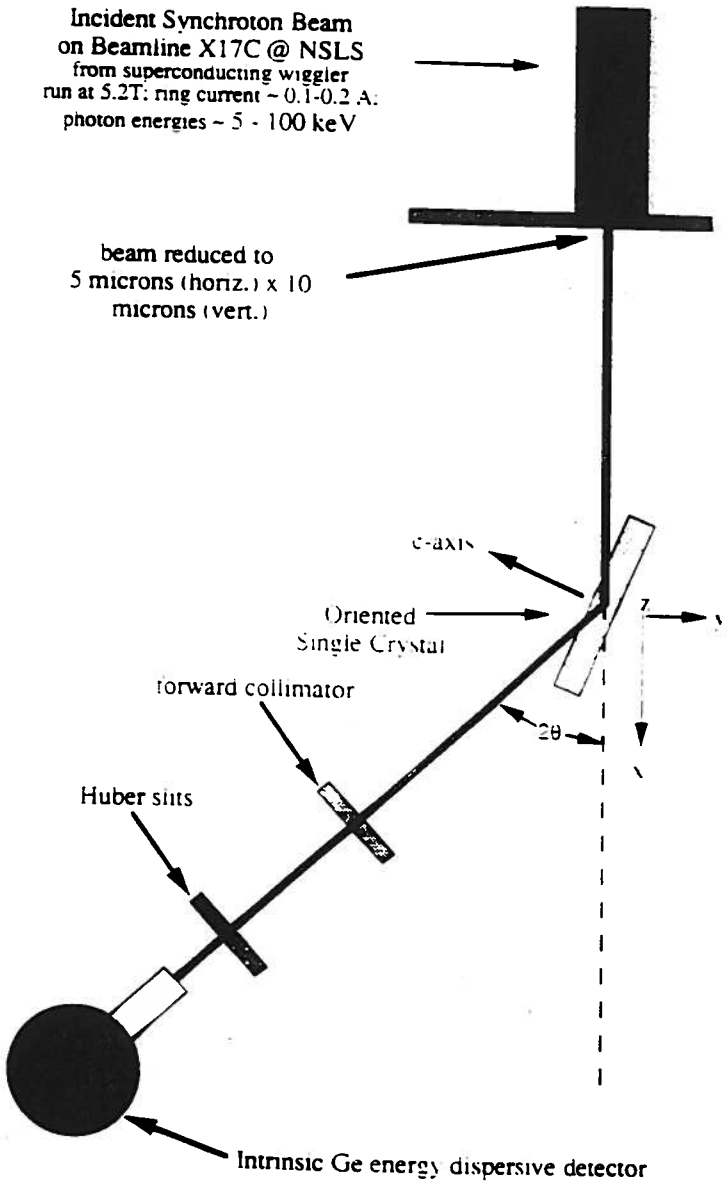

Fig. 1. Schematic drawing of the set-up for the energy dispersive diffraction measurements (top view).

Each crystal was illuminated with unfiltered, polychromatic radiation emerging from the wiggler magnet (operated at 5.2 T) and restricted spatially, as detailed above. The scattered x-rays were analyzed at a fixed diffraction angle, 2θ, typically about 13°, as a function of energy with an intrinsic Ge energy sensitive detector. The exact 2θ-position of the detector was determined separately for each experiment using a gold calibration foil in place of the sample. Once an experiment was started, only the sample moved; all other elements of the system remained stationary. A typical diffraction spectrum for the $(0,0,\ell)$-class of reflections for a $YBa_2Cu_3O_{7-\delta}$ crystal is shown in Fig. 2. The diffraction peaks are superimposed on a background that is the convolution of the energy-intensity profile of the radiation on this beamline and the response of the photon detection system. The peaks labeled, "e", are Ge-escape peaks.

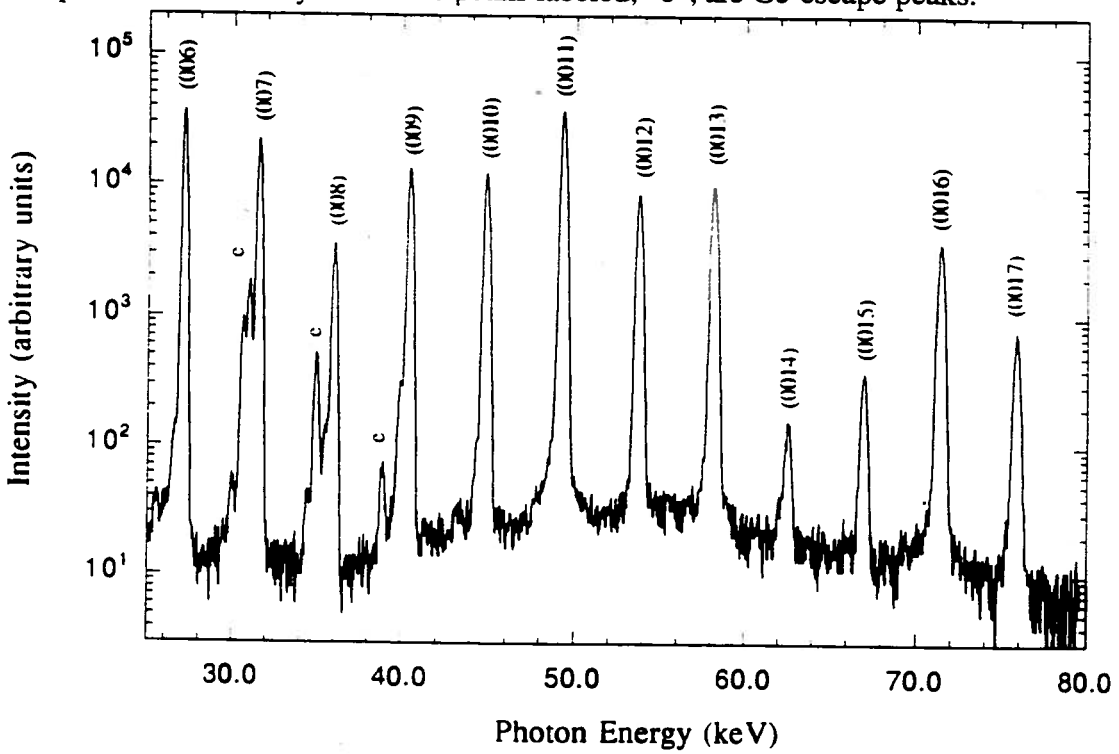

Fig. 2. Energy-dispersive diffraction spectrum of the (0.0.ℓ) class of reflections recorded from a $YBa_2Cu_3O_{7-\delta}$ crystal.

Data were collected in one of two methods. In Procedure #1, complete spectra were recorded as a function of z, in steps ranging in size from 2 to 100 μm, from the one edge of the crystal to the other. At each position, the $(0,0,\ell)$ peak of interest, usually the (00,11) or (00,13), was automatically centered in ω and χ and then the spectrum recorded. This procedure then was repeated at various settings in y. Alternatively, in Procedure #2, data were recorded by automatically transitioning in (y,z) to a new position, then centering the peak of interest, usually the (00,11), and collecting data in the vicinity of this peak only, as the crystal was stepped in ω through the peak.

In both cases, least-square fits were then made to the spectra to determine the center, height, and width of the Bragg peak under study. (The peak heights were corrected for variations in the synchrotron ring current. The energy-channel number calibration curve for the multichannel analyzer was determined using an assortment of known x-ray fluorescence peaks.) The photon energy associated with the center of the measured peak, E_ℓ, was then used to determine the length of the c-axis from the Bragg relation:

$$c = \frac{\lambda \kappa}{2 E_\lambda \sin \theta} \qquad [1]$$

where κ is equal to the product of Planck's constant and the speed of light. Except for the measurements on $Nd_{2-x}Ce_xCuO_{4-y}$, all other studies were on $YBa_2Cu_3O_{7-\delta}$ single crystals and an ordered thin film grown by a variety of methods. It is well established that the *c*-axis length of the orthorhombic unit cell of these compounds is a reliable indicator the oxygen content, 7-δ. The following relation was used to relate the length of the *c*-axis to the oxygen content:[1] (This relation does not necessarily hold for thin films.)

$$(7 - \delta) = 74.49 - 5.787\, c \qquad [2]$$

where *c* is in Å and 7-δ represents the number of oxygen atoms in the formula unit, $YBa_2Cu_3O_{7-\delta}$.

3. RESULTS AND DISCUSSIONS

The objective of the work reported in this paper was to survey a number of HTS single crystals, prepared by a variety of growth methods, and assess their degree of uniformity and homogeneity. To this end, one crystal of $Nd_{2-x}Ce_xCuO_{4-y}$, three crystals and a thin film of $YBa_2Cu_3O_{7-\delta}$ were studied. Each was prepared by a different growth procedure and crystal growing group. Details of how the various crystals were prepared will be given in a future publication.

3.1 $Nd_{2-x}Ce_xCuO_{4-y}$

The $Ln_{2-x}M_xCuO_{4-y}$ family of superconductors is unique among the cuprates because of the unusual symmetry in the doping characteristics between hole and electron carrier materials. Tetravalent doping ($M=Ce^{4+}$: Ln = Pr, Nd, Sm, Eu) produces the electron carrier material ($T_c \approx 20$ K) for the range of compositions ($0.14 < x < 0.18$). The production of optimal samples for superconductivity is further complicated by the need for a small oxygen defect ($y \approx 0.02$), usually produced by a high temperature anneal in an inert atmosphere. There are many reports of mixed phase behavior in the Nd-Ce-Cu-O system. This phenomenon is usually attributed to inhomogeneities in the oxygen content, though recently inhomogeneities in the Ce concentrations have been described.[2] Drews et al.[3] studied thick single crystals of $Nd_{2-x}Ce_xCuO_{4-y}$ and found clear evidence for phase segregation in the form of sheets of stoichiometric material in the *ab*-plane with varying Ce concentration. Although prior investigators usually have restricted their attention to thin crystals (< 30 μm) which show sharp superconducting transitions and BCS-like behavior, an appreciation of the difficulties present in thicker samples is important.

The following is a summary of a more detailed report previously published on this sample.[4] Optical microscopic analyses of a polished cross-section of the crystal provided evidence of an unusual morphology. When viewed between crossed polarizers, variable contrast was observed in the form of stacked layers of material in the *a-b* plane. Four major layers were clearly visible, separated by apparently sharp boundaries without cracks or flux inclusions. Scanning electron microscopy (SEM) coupled with energy dispersive x-ray spectroscopy (EDXS) measurements across the polished section indicated that the observed optical contrast correlated with a variation in the measured Ce concentration. The two inner layers have similar Ce concentrations corresponding to x = 0.19, while the two outer layers had Ce concentrations corresponding to x = 0.16 and x = 0.13 AC magnetic susceptibility measured with either orientation of the crystal relative to the pick-up coil shows distinct transitions at 24 and 20 K. The double transitions can be explained if the outer layers correspond to the lower T_c material. Details are given in Refs. 5 and 6.

Standard diffraction measurements of the (0,0,6) and (0,0, $\bar{6}$) reflections made on a four-circle diffractometer using Cu Kα radiation confirmed that the *c*-axis lattice parameter was different for each face of the crystal; measured values were 12.082 ± 0.004 Å and 12.118 ± 0.001 Å. Based on published powder diffraction studies of this system, these lattice parameters correspond to Ce concentrations of x = 0.09 and x = 0.15, respectively.[7] The interesting morphology of this sample suggested that it would represent an ideal candidate for study using the high energy x-ray micro-probe at NSLS.

Spectra were recorded as a function of the y-position every 10 μm for three different *x*-positions (*x* = 0, 50, and 150 μm). In this case, the peak energies for the even-order (0,0,ℓ)-reflections were measured (mixed order reflections are excluded by symmetry for this structure) and used to calculate the *c*-axis lattice parameter.

The results from these measurements are shown in Fig. 3. We note the similarity in relative variation of *c*-axis parameter with our earlier measurements of Ce variation by EDXS. The errors in the calculated *c*-axis lattice parameter for our NSLS measurements are typically ±0.01 Å. There is a general similarity of shape in the Ce content variation across the edge of the crystal as measured by EDXS, and the variation of *c*-axis parameter measured at NSLS. If the variation in the *c*-axis is interpreted as a variation of Ce content, according to the dependence determined by Takagi et al.,[8] then the data show a variation from x = 0.12 at one face, to x = 0.16 for the interior region, to x = 0.07 near the opposite face. This is similar to the variation determined by EDXS. Micro-structural variations on the scale of 10 or 20 μm are clearly visible in the *c*-axis.

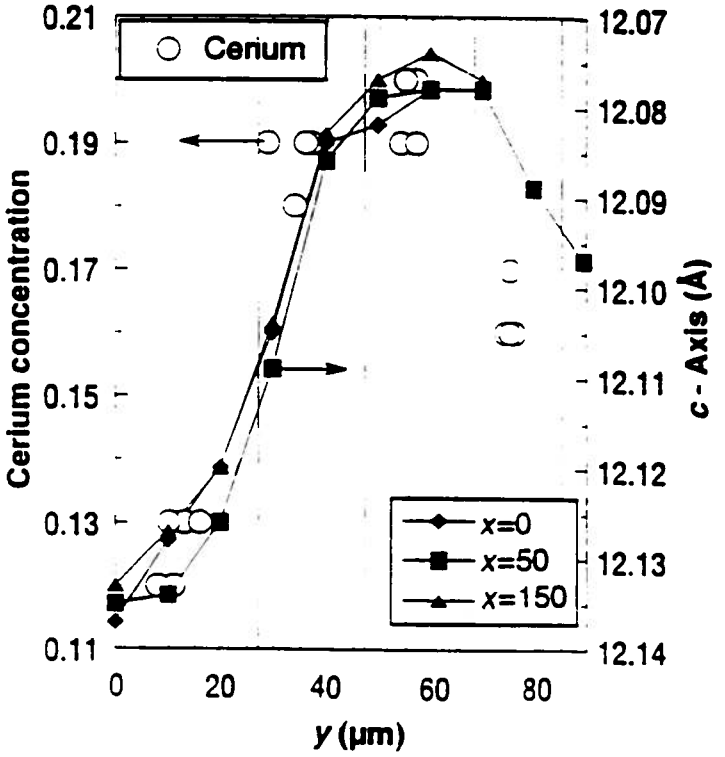

Fig. 3. Variation of the Ce content (o) as determined from the Ce-fluorescence peak and the *c*-axis lattice parameter as determined from the micro-diffraction measurements, each as a function of *y*.

3.1 $YBa_2Cu_3O_{7-\delta}$ - Crystal No. 1

Measurements on the first $YBa_2Cu_3O_{7-\delta}$ (YBCO) crystal also were reported previously.[9] A summary follows: Three separate z-scans were performed. The first was made with the beam passing through the central region of the crystal (*y* = 0), the second with the *y*-position of the sample increased 20 μm, and the third with *y* increased an additional 10 μm. The edge of the sample in this direction, as measured with the x-ray beam, was at *y* = 36 μm. So the last scan (*y* = 30 μm) came from an area that was about 6 μm from the lateral face of the crystal. The results are plotted in Fig. 4.

The most striking feature of each scan is the precipitous change in 7-δ near the edges as the crystal moves into and out of the beam. The value of 7-δ is relatively constant, to within the scatter in the data, throughout

the central region, but falls off significantly on either end. For the scan taken closest to the lateral face (y = 30 μm), 7-δ is also reduced. The implication is that, whereas the oxygen content is relatively constant throughout the bulk, it appears to drop off near the surfaces, as if oxygen had "leaked" out of the sample.

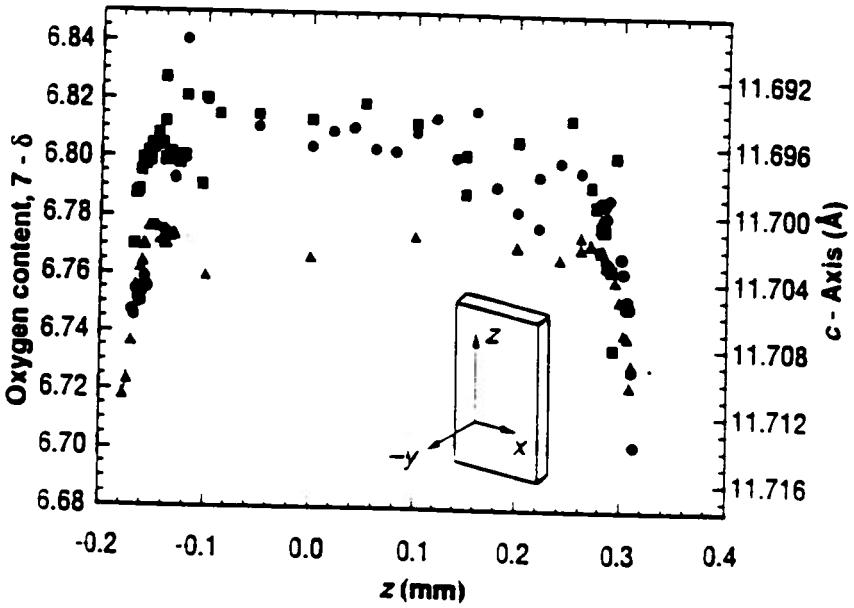

Fig. 4. Variation of the oxygen parameter, (7-δ), and the c-axis lattice parameter, both as a function of z, along the length of YBCO - Crystal No. 1. Scans were made along three different y-settings: circles at y = 0.00 μm, near the center of the crystal; squares at y = 20 μm, closer to the lateral face; and triangles at y = 30 μm, within about 6 μm of the face surface. The orientation of the crystal is shown in the inset.

As a reference, these same data also are plotted in Fig. 5 as a function of the fractional change in the c-axis lattice parameter.

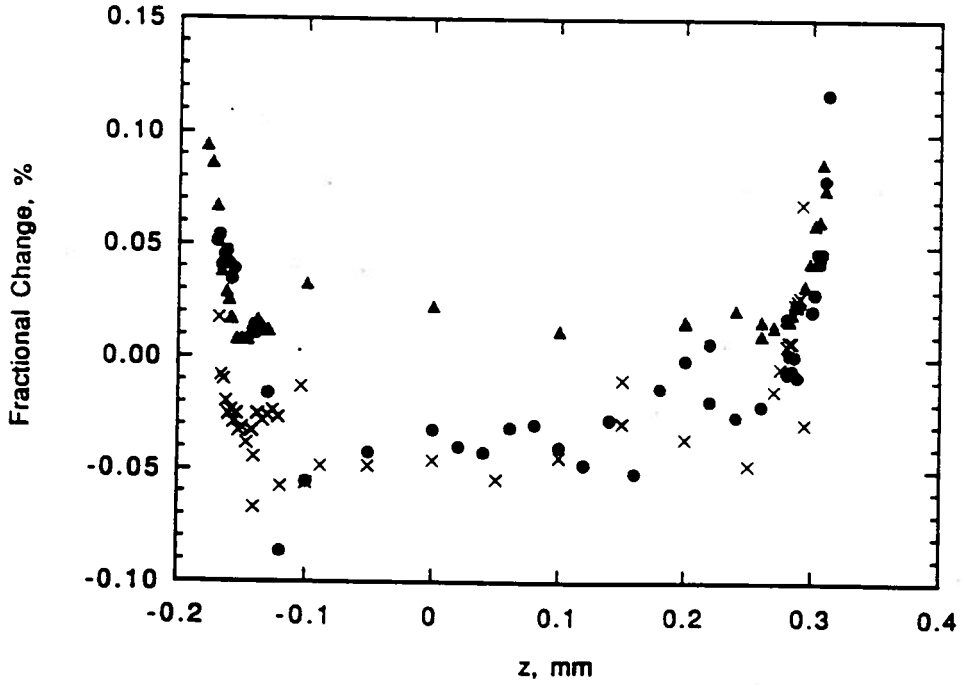

Fig. 5. Fractional change in the c-axis lattice parameter as a function of z, along the length of YBCO - Crystal No. 1. (Same data as in Fig. 4)

3.2 $YBa_2Cu_3O_{7-\delta}$ - Crystal No. 2 and Thin Film

Fractional changes in the lattice parameter are shown in Figs. 6 and 7 for a different YBCO single crystal and thin film, respectively. The thin film was grown on single crystal substrate of MgO. To avoid saturation of the x-ray detector that would be caused by diffraction from the MgO, for the thin film, the (0,1,9)-reflection was measured. In both cases, there is about a 0.15% scatter in the data, but no systematic change, similar to that seen in Crystal No. 1.

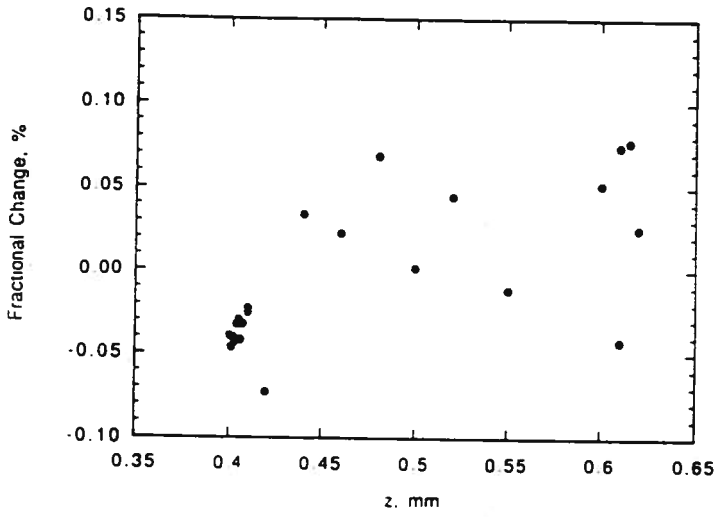

Fig. 6. Fractional change in c for YBCO Crystal No. 2

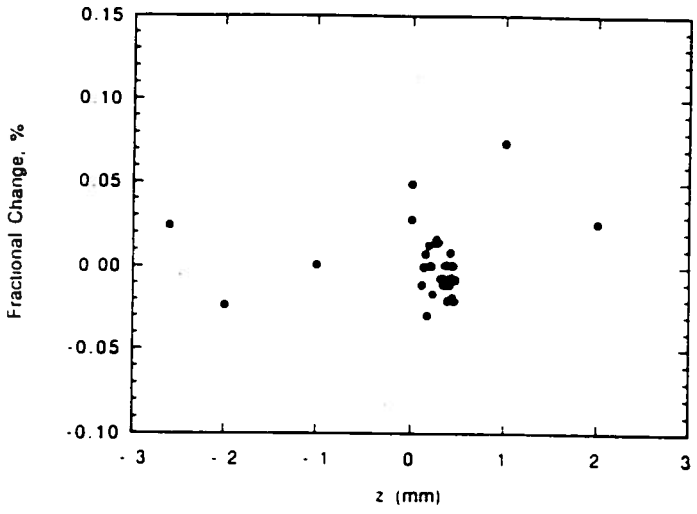

Fig. 7. Fractional change in $d(0,1,9)$ for a thin film of YBCO

3.3 $YBa_2Cu_3O_{7-\delta}$ - Crystal No. 3

The third crystal of $YBa_2Cu_3O_{7-\delta}$ was examined only along one 10 μm wide path near the center of its approximate 1 mm length. The measured fractional change in the c-axis along this path are shown in Fig. 8.

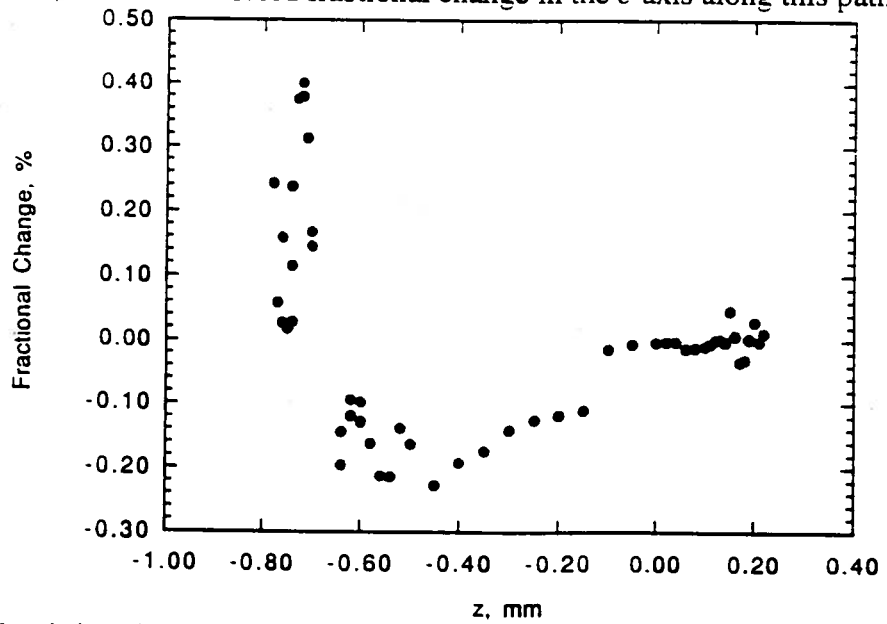

Fig. 8. Fractional variation of the c-axis lattice parameter as a function of z along the length of YBCO - Crystal No. 3.

On one end, an increase in the lattice parameter is seen, similar to that seen in Crystal No. 1, but on the other end, there is no observable change. The implication of this is that the oxygen decreases near one edge, but not the other. Also of interest is the internal anomaly seen at about z = -0.5. A more detailed examination of this revealed a significant change in the intensity of the (00,11) diffraction peak through the material. This is exhibited in Fig. 9. (Some of the spikes in Fig. 9 are an artifact of the plotting program.) In the central region of the crystal, the intensity of the (00,11) peak is two orders of magnitude weaker than near either end. It is nevertheless, a single, well defined peak. Near the each end however, the single (00,11)-peak splits into a doublet, and near the lower end ($-0.80 \leq z \leq -0.50$) the center of this doublet is seen to shift in ω. There is also the appearance of a weak third peak in this region. The implication of all this is that this crystal is not single and homogeneous through the region scanned.

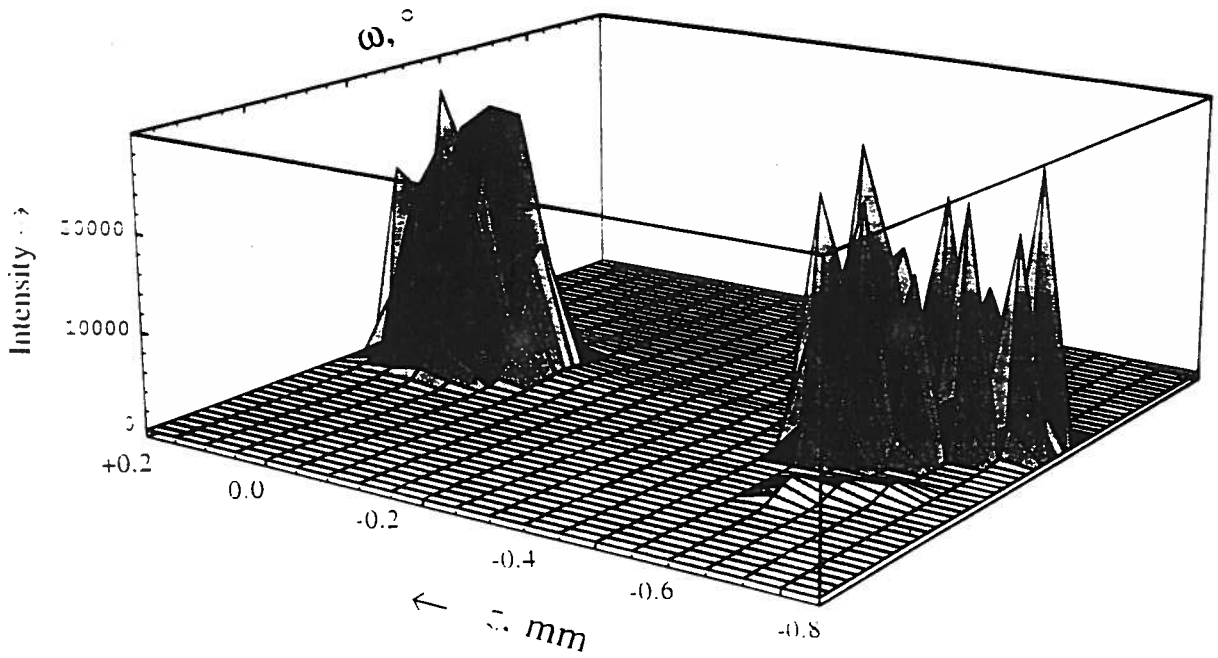

Fig. 9. Intensity of the (00.11)-peak of YBCO - Crystal No. 3 measured as a function of ω. systematically from one end of the crystal to the other ($-0.80 \leq z \leq +0.20$)

3.2 $YBa_2Cu_3O_{7-\delta}$ - Crystal No. 4

The fourth crystal of YBCO was systematically examined according to Procedure #2. The results of three scans in z, made at y positions of 0.10, 0.15, and 0.20 mm are shown in Fig. 10. Each of the three scans shows approximately the same effect. A gentle change in the oxygen content from about 6.9 at one end to about 6.8 at the other. All the diffraction peaks recorded from this sample were singlets and of generally constant intensity.

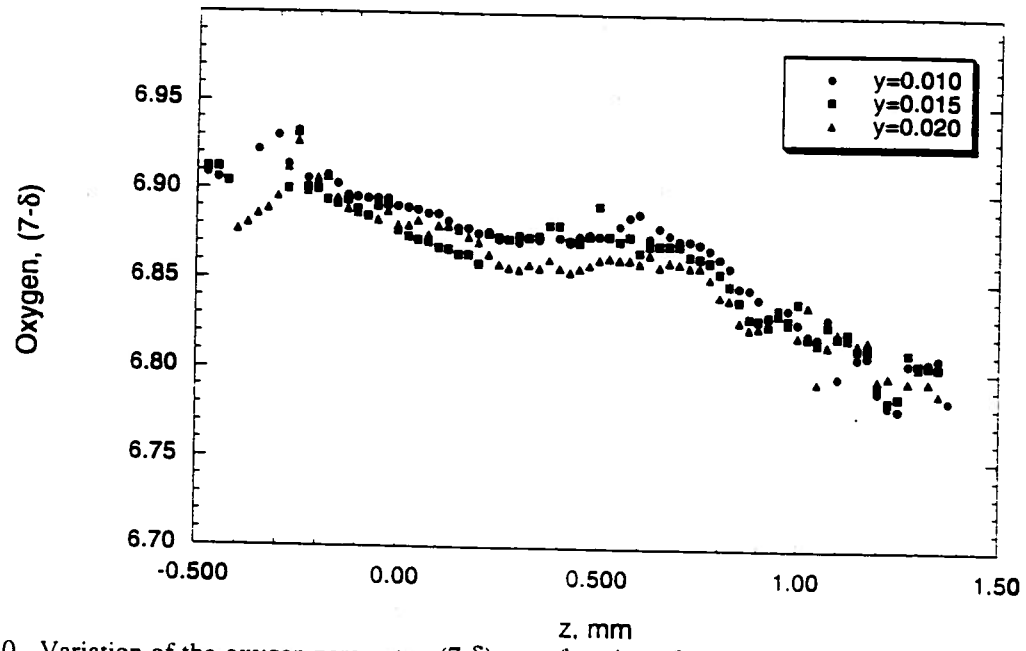

Fig. 10. Variation of the oxygen parameter, (7-δ), as a function of z, along the length of $YBa_2Cu_3O_{7-\delta}$ - Crystal No. 4. Scans were made along three different y-settings: circles at y = 10 μm; squares at y = 15 μm, triangles at y = 20 μm.

4. CONCLUSIONS

These observations provide direct evidence of structural variations on length scales of tens of microns. The superconductors examined in this investigation were probed with an extremely intense x-ray beam of only 5 x 10 μm in cross section. For all samples, the data reveal small structural variations on a spatial scale of 10 to 20 μm, heretofore not seen. For the $YBa_2Cu_3O_{7-\delta}$, the observed effect is believed to be due to changes in oxygen. In the case of $Nd_{2-x}Ce_xCuO_{4-y}$, the observed structural variances are interpreted in terms of changes in the Ce content. These results emphasize the need for caution in interpreting experimental results for HTS.

There are two length scales which characterize the superconducting state, the penetration depth, λ, and the coherence length, ξ. In HTS, both are highly anisotropic and change by an order of magnitude in going from the *ab*-plane to the *c*-direction. At 0 K, λ_{ab} is of the order of 1000 Å, whereas λ_c is ten times greater; ξ_{ab} is of the order of 10 Å, whereas ξ_c is only one-tenth as large. Although the length scales probed here are large compared to these values, the observed inhomogeneities are big enough to alter the properties measured in standard measurements. In particular, experiments which depend on clean surfaces with uniform, ideal, superconducting properties, such as penetration depth and tunneling, will be affected strongly by such structural features. This may be particularly true for $YBa_2Cu_3O_{7-\delta}$ crystals.[10] On the other hand, thin $Nd_{2-x}Ce_xCuO_{4-y}$ crystals (< 20 μm) exhibit no evidence of structural inhomogeneities. This point is highlighted by tunneling and penetration depth measurements on thin, single phase $Nd_{2-x}Ce_xCuO_{4-y}$ crystals which produce results consistent with BCS-theory.[11,12]

As we strive to achieve smaller beam sizes, we are likely to observe significant structural defects in sub-μm length scales. Ideally, as our spatial resolution increases, we will be able to answer more subtle questions regarding the nature of the defect structures and their origins.

5. REFERENCES

† National Science Foundation Science and Technology Center

1. T. A. Vanderah, C. K. Lowe-Ma, D. E. Bliss, M. W. Decker, M. S. Osofsky, E. F. Skelton, and M. M. Miller, J. Cryst. Growth **118**, 385-395 (1992)
2. W. Sadowski et al., J. Less Common Metals **164 & 165**, 824-831 (1990).
3. Drews et al., Physica C **200**, 122-128 (1992)
4. E. F. Skelton, A. R. Drews, M. S. Osofsky, S. B. Qadri, J. Z. Hu, T. A. Vanderah, J. L. Peng, and R. L. Greene, Science **263**, 1416-1418 (1994).
5. M. S. Osofsky, J. L. Cohn, E. F. Skelton, M. M. Miller, R. J. Soulen, Jr., S. A. Wolf, and T. A. Vanderah, Phys. Rev. B **45**, 4916 (1992).
6. M. E. Parks, A. Navrotsky, K. Mocala, E. Takayama-Muromachi, A. Jacobson, and P. K. Davies, J. Solid State Chem. **79**, 53 (1989).
7. H. Takagi, S. Uchida, and Y. Tokura, Phys. Rev. Lett. **62**(10) 1197-1200 (1989).
8. *Ibid.*
9. E. F. Skelton, et al., Science **263**, 1416-1418 (1994).
10. W. N. Hardy, D. A. Bonn, D. C. Morgan, R. Liang, and K. Zhang, Phys. Rev. Lett. **70**, 3999 (1993).
11. S. M. Anlage, D. H. Wu, J. Mao, Sining Mao, X. X. Xi, T. Venkatesan, J. L. Peng, and R. L. Greene, Phys. Rev. B **50**, 523 (1994); and refs. therein.
12. Q. Huang, J. F. Zasadzinski, N. Talhawala, K. E. Gray, D. G. Hinks, J. L. Peng, and R. L. Greene, Nature **347**, 369 (1990)